

Reduced-Order Models for Electromagnetic Scattering Problems

Amit Hochman, *Member, IEEE*, Jorge Fernández Villena, Athanasios G. Polimeridis, *Member, IEEE*, Luís Miguel Silveira, *Fellow, IEEE*, Jacob K. White, *Fellow, IEEE*, and Luca Daniel

Abstract—We consider model-order reduction of systems occurring in electromagnetic scattering problems, where the inputs are current distributions operating in the presence of a scatterer, and the outputs are their corresponding scattered fields. Using the singular-value decomposition (SVD), we formally derive minimal-order models for such systems. We then use a discrete empirical interpolation method (DEIM) to render the minimal-order models more suitable to numerical computation. These models consist of a set of elementary sources and a set of observation points, both interior to the scatterer, and located automatically by the DEIM. A single matrix then maps the values of any incident field at the observation points to the amplitudes of the sources needed to approximate the corresponding scattered field. Similar to a Green's function, these models can be used to quickly analyze the interaction of the scatterer with other nearby scatterers or antennas.

Index Terms—Electromagnetic scattering, integral equations, modeling.

I. INTRODUCTION

THE AIM in model-order reduction (MOR) is to replace a complicated system by a simpler one, while preserving the input–output relationship of the former. Typically, the systems are dynamical systems, and MOR is used to generate models that can be integrated in system-level time-domain simulations [1]–[3]. For example, MOR is routinely used to generate compact models for microwave components from detailed simulations or measurements [4], [5].

An extension of MOR, parametric MOR, can be used to construct models that remain accurate for a range of material and geometric parameters [6]–[8]. For example, in [6], waveguide fields for a range of frequencies and permeabilities are approximated using a weighted combination of representative field solutions obtained at a small set of frequencies and permeabili-

Manuscript received July 18, 2013; revised December 22, 2013; accepted February 22, 2014. Date of publication April 01, 2014; date of current version May 29, 2014. This work was supported in part by the Swiss National Science Foundation under Grant PA00P2-142060, in part by national funds through FCT under contract PEst-OE/EEI/LA0021/2013, in part by grants from the Singapore-MIT programs in Computational Engineering and in Computational and Systems Biology, and in part by grants from the Skolkovo-MIT initiative in Computational Mathematics.

A. Hochman, J. F. Villena, A. G. Polimeridis, J. K. White, and L. Daniel are with the Research Laboratory of Electronics, Department of Electrical Engineering and Computer Science, Massachusetts Institute of Technology, Cambridge, MA 02139 USA (e-mail: jvillena@mit.edu).

L. M. Silveira is with the Instituto de Engenharia de Sistemas e Computadores, Investigação e Desenvolvimento em Lisboa (INESC ID), Lisbon 1000-029, Portugal and also with Instituto Superior Técnico (IST), Technical University of Lisbon, Lisbon 1000-049, Portugal.

Color versions of one or more of the figures in this paper are available online at <http://ieeexplore.ieee.org>.

Digital Object Identifier 10.1109/TAP.2014.2314734

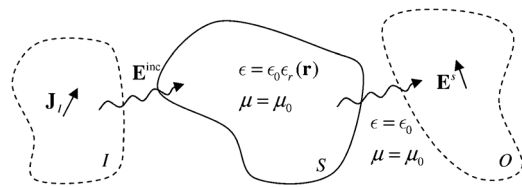


Fig. 1. Input region I , an inhomogeneous dielectric scatterer S and an output region O .

ties. To determine the weights, a low-order equation is derived for them, by Galerkin projection of the relevant high-order discretized partial differential equations.

In this paper, we borrow from the MOR framework to generate ROMs for electromagnetic scattering problems. However, we only consider time-harmonic fields (with an $\exp(j\omega t)$ time dependence) and not any time-domain dynamical system. Also, while the inputs and outputs usually considered in MOR are port amplitudes, our inputs and outputs are, respectively, current distributions and fields. Hence, while ideas from MOR underlie much of this work, the premises are different.

We consider the situation depicted in Fig. 1, where we have a scatterer occupying region S , an input region I , where currents may reside, and an output region O , where the scattered field may be observed. Regions I and O may intersect, may be identical, and may be infinite, but they may not have any point in common with S . Our goal is to obtain an ROM for the system relating the currents in region I to the scattered field in region O . To achieve this goal, we rely on the availability of a (presumably time-consuming) routine for solving the scattering problem and yielding the output for an arbitrary input. This routine is to be used in an offline, model-generation stage, and the pertinent questions are then how to choose its inputs and how to use the corresponding outputs to generate the read-only memory (ROM).

For concreteness, we assume that the scatterer is an inhomogeneous dielectric, the currents in region I are electric, and the field to be observed in region O is the scattered electric field. Other scattering problems, such as those involving magnetic materials or perfect conductors, could be handled similarly. The system relating the inputs to the outputs can be written as follows:

$$\text{Input : } \mathbf{E}^{\text{inc}} = \mathcal{K}_I(\mathbf{J}_I) \quad (1)$$

$$\text{State equation : } \mathcal{L}(\mathbf{J}_S) = \mathbf{E}^{\text{inc}} \quad (2)$$

$$\text{Output : } \mathbf{E}^{\text{scat}} = \mathcal{K}_O(\mathbf{J}_S) \quad (3)$$

where the \mathcal{K}_I operator maps \mathbf{J}_I , a current in region I , to the electric field it produces in free space, evaluated at observation

points in region S . The field $\mathcal{K}_I(\mathbf{J}_I)$ is also denoted \mathbf{E}^{inc} since it is an incident field that induces an electric polarization current \mathbf{J}_S in the scatterer region S . The operator \mathcal{L} maps \mathbf{J}_S , a current in region S , to an incident field that would induce it on the scatterer, essentially, it is the impedance operator to be inverted in the course of solving the scattering problem. Finally, the \mathcal{K}_O operator maps a current in region S to the electric field it produces in free space, evaluated at observation points in region O , that is, it yields the scattered electric field, \mathbf{E}^{scat} . While the operator \mathcal{L} is typically time-consuming to apply, and the \mathcal{K}_I and \mathcal{K}_O operators can be applied fast by using fast-multipole or similar methods, since they are just integral operators with the free-space dyadic Green's function as kernel.

The system formulation (1)–(3) is useful for considering the choice of inputs for the offline stage. A natural choice might be to choose the inputs so that the fields incident on the scatterer span the range of the operator \mathcal{K}_I . Since we are assuming that regions I and S are distinct, this operator is compact. This implies it has a finite numerical rank, and this rank is an upperbound on the required number of inputs. Clearly, if we precompute the response to all of these inputs, the response to an arbitrary input will be obtainable as a weighted combination of the precomputed responses.

As natural as this choice may be, it typically involves more inputs than necessary. The reason is that the numerical rank of the operator

$$\mathcal{T} = \mathcal{K}_O \mathcal{L}^{-1} \mathcal{K}_I \quad (4)$$

which maps the inputs to the outputs is never larger, and typically smaller, than that of \mathcal{K}_I alone. Since \mathcal{K}_O is also a compact operator, so is $\mathcal{K}_O \mathcal{L}^{-1}$. It therefore has an approximate null-space, and certain vectors in the range of \mathcal{K}_I could fall in this approximate null space. Physically, this can occur if, for example, the output region includes a null in a bistatic radar cross section of the scatterer.

The compactness of \mathcal{K}_I and \mathcal{K}_O hinges on our assumption that regions I and O do not intersect with S . If both regions I and O include many points that are very close to region S , the reduction in order may be limited. Regardless, the reduction will be close to optimal, as we now explain.

A minimal set of inputs needed to generate a model of \mathcal{T} with a prescribed L_2 error is readily obtained from an SVD of \mathcal{T}

$$\mathcal{T}(\mathbf{J}) = \sum_{i=1}^{\infty} \mathbf{u}_i \sigma_i (\mathbf{v}_i, \mathbf{J})_I. \quad (5)$$

In (5), the \mathbf{u}_i and \mathbf{v}_i are the left and right singular vectors, respectively, the σ_i are the singular values (positive and ordered in decreasing order), and the inner product is given by

$$(\mathbf{u}, \mathbf{v})_I = \int_I \overline{\mathbf{u}(\mathbf{r})} \cdot \mathbf{v}(\mathbf{r}) d\mathbf{v} \quad (6)$$

where the overbar denotes the complex conjugate. Note that an SVD exists if and only if an operator is compact. While \mathcal{L}^{-1} is not compact, surrounding it with the compact operators \mathcal{K}_I and \mathcal{K}_O yields the compact operator \mathcal{T} . By truncating (5), an ROM is readily obtained, and its order say m is minimal for a certain

L_2 error criterion. The first k of the \mathbf{v}_i are the inputs for which the responses \mathbf{u}_i should be precomputed.

The aforementioned observation provides a formal guideline for choosing the inputs for the offline stage, but it is still unclear how to determine these inputs in practice. In this paper, we develop a computational scheme for this problem, where we do not compute the singular vectors explicitly, but show how to work with the SVD representation implicitly. The computational scheme makes use of two relatively new numerical techniques: randomized SVD (RSVD) algorithms and the discrete empirical interpolation method (DEIM) [9]–[11], and the observation that it is easy to form approximate SVDs of \mathcal{K}_I and \mathcal{K}_O . The final result is a model for \mathcal{T} which consists of $r_O = O(m)$ fictitious elementary sources inside the scatterer, at locations chosen automatically by the algorithm. The amplitudes of the sources required to approximate the scattered field are obtained by evaluating the incident field at a second set of $r_I = O(m)$ points inside the scatterer and multiplying by an $r_O \times r_I$ matrix. Assuming r_I and r_O are small enough, this model allows rapid evaluation of the scattered field in region O for an arbitrary incident field due to sources in region I .

The idea of modeling a scatterer by precomputing the response to a set of excitations is not new of course. When spherical waves are used as excitations, one obtains the classical scattering matrix, which is best suited to approximately spherical scatterers of moderate electrical sizes. For arbitrarily shaped scatterers, the characteristic modes introduced by Garbacz [12] and Harrington and Mautz [13] are a natural generalization of the scattering matrix approach. The excitations used in this paper may be considered as a further generalization, one that obtains whether information regarding the possible input and output regions is taken into account.

Tailoring the excitations to the input and output regions can be useful in antenna siting problems, where antennas are to be mounted on a complex scatterer (say, an aircraft), but their possible locations are highly constrained. Then, the number of modes needed to represent the input–output relationship between the potential antenna sites is determined more by the number of potential sites and their size, than by the size of the scatterer. Hence, the number of modes may be greatly reduced compared to the number needed for a more general analysis.

For an extreme example, if both regions contain only a single point, then, regardless of the complexity of the scatterer, the linear relationship between input and output requires a single number for its specification (at a single frequency). If instead of single-point regions, we have a few points in each region, then a small matrix suffices to specify the input–output relation. Finally, if the regions contain many closely spaced points, then the corresponding matrix will be large, but will be close in norm to a matrix of low rank. Regardless of the regions, an SVD of the input–output matrix can be used to generate a model of minimal rank for a prescribed L_2 error.

In this paper, we consider an example which demonstrates the usefulness of the aforementioned approach. We generate an ROM for a realistic model of a human head, for a magnetic resonance imaging (MRI) application. In this example, the design of antennas for radio-frequency excitation of the head is very time-consuming, because the presence of the head influences

the current distribution on the antennas. Hence, any simulation of the coils must include the head model. However, the location of the antennas is restricted to a thin shell around the head model, and this is exploited by our approach to obtain a compact ROM that can be used to simulate a given antenna configuration very quickly.

Suppose we model a given antenna configuration using the method of moments (MoM). Then, the impedance matrix for the antennas in the presence of the head is written as the sum of a free-space matrix Z_0 and a perturbation due to the presence of the scatterer Z_s . The first matrix is the usual MoM matrix that can be evaluated by standard codes, or applied fast with a fast matrix-vector product technique. The second matrix is obtained by using the ROM, and it is, by construction, given in factored form that enables a fast matrix-vector product. Let G denote the $r_I \times N_A$ matrix that maps the N_A basis functions used to model currents in the antennas to the fields they produce, in free space, at the r_I points in the ROM model. Let A denote the $r_I \times r_I$ matrix of the ROM (in this case, $r_I = r_O$). Then for Z_s , we have

$$Z_s = G^T A G. \quad (7)$$

Assuming r_I is not too large, this form can be used to apply Z_s quickly for an iterative solver, or if N_A is not too large, Z_s can be computed explicitly and a direct solver can be used. In this case, the most time-consuming operation is filling the MoM matrices, which usually requires evaluating N_A^2 Galerkin integrals. However, for Z_s , we only need the fields of N_A basis functions at r_I points, so, assuming $r_I \approx N_A$, the cost of filling Z_s is similar to the cost of filling Z_0 . Therefore, analyzing a given antenna configuration in the presence of the head can be performed with standard MoM codes, and with a computational cost that is only slightly larger than that of a free-space analysis. In this respect, the ROM is equivalent to a numerically computed Green's function for the scatterer.

The form of the ROMs we obtain is closely related to the generalized scattering matrix (GSM) of [14] and [15]. Here too, fields due to elementary sources inside a scatterer are used to represent the scattered field, and their amplitudes are linearly related to the values of an incident field evaluated at a set of points. Our work is different in a few significant respects however. In [14] and [15], the sets of inputs chosen for precomputation are elementary sources placed on a curve (these works are for 2-D) outside the scatterer. In [15], the SVD is used to determine how many inputs are necessary, but the analysis is based on the range of \mathcal{K}_I , not on the SVD of \mathcal{T} . Also, the sources inside the scatterer are distributed uniformly on a curve conformal with the scatterer boundary, whereas we distribute them at the DEIM points, which can be anywhere on a fairly dense grid inside the scatterer. While placing sources on a curve yields a complete set of basis functions, our set is overcomplete and this may yield more compact models (for a fuller discussion of this point, see [16]).

Another related method is the synthetic-functions expansion (SFX) [17]. This is a domain-decomposition approach, where a large scatterer is partitioned into smaller scatterers, and basis functions are obtained for each of the smaller scatterers by ex-

citing them with various excitations. For example, if the smaller scatterers are well-separated, the excitations are due to elementary sources on a surface enclosing the smaller scatterer. Here, too, the SVD is used to determine the number of elementary sources needed to approximate an arbitrary function in the range of \mathcal{K}_I .

Finally, though the aim of our method is different, it shares some similarities with the technique of [18], recently proposed for inverse-scattering problems, as well as the adaptive cross approximation (ACA) [19]–[21], where the coupling between well-separated regions is approximated using low-rank matrices.

Notation: We follow the convention that column vectors are denoted by lowercase symbols and matrices by uppercase symbols. Scalars are typically lowercase, though we use N_x to denote the number of elements in vectors and matrices. Bold symbols are used for physical vector fields. Operators mapping to physical vector fields are denoted by calligraphic symbols, while those mapping to a column vector are denoted by lowercase symbols.

The remainder of this paper is organized as follows. We begin by describing how the SVD of the operator \mathcal{T} can be computed (Section II). Then, we explain how to expedite the computation of time-consuming inner products in this SVD, using the DEIM (Section IV-B). In Section IV, we discuss implementation issues, and in Section V, we show numerical results for an example pertinent to MRI. Finally, the paper is summarized in Section VI.

II. CONSTRUCTING THE ROM

Our ROMs are based on an SVD of the operator \mathcal{T} , formally given by (5). This representation is attractive because if the series is truncated after m terms, the resulting model is an optimal rank- m approximation of the operator, with respect to an L_2 error criterion. The main difficulty with this idea is that the \mathbf{v}_i and the \mathbf{u}_i have to be known throughout the input and output regions, respectively, and, in general, these regions are 3-D, and potentially infinite. Our approach for this problem is to shift computations from regions I and O to region S , in a manner reminiscent of the reciprocity theorem. For example, instead of computing inner products between a source in region I and the \mathbf{v}_i , we compute inner products between the fields that the source generates in region S , and a set of corresponding distributions in region S . Computing inner products in region S is much easier, since the fields are smoother than their sources, the region is finite, and we can make use of the basis functions of whichever solver we employ. To find these corresponding distributions, we write the SVD of \mathcal{T} using the SVDs of \mathcal{K}_I and \mathcal{K}_O .

Let us first define these operators more precisely. The operator \mathcal{K}_I maps currents in region I to the electric fields they generate in region S . It is given by

$$\mathcal{K}_I(\mathbf{J}) = \int_I \mathbf{G}(\mathbf{r} - \mathbf{r}') \cdot \mathbf{J}(\mathbf{r}') dv', \quad \mathbf{r} \in S \quad (8)$$

where \mathbf{G} is the free-space dyadic Green's function

$$\mathbf{G}(\mathbf{r}) = -j\omega\mu_0 \left[\mathbf{I} + \frac{\nabla\nabla}{k_0^2} \right] \frac{e^{-jk_0|\mathbf{r}|}}{4\pi|\mathbf{r}|}. \quad (9)$$

Here, μ_0 is the free-space permeability, \mathbf{I} the identity dyadic, and $k_0 = \omega/c$, with c being the speed of light in vacuum. Similarly, the operator \mathcal{K}_O maps currents in region S to the electric fields they generate in region O . It is given by

$$\mathcal{K}_O(\mathbf{J}) = \int_S \mathbf{G}(\mathbf{r} - \mathbf{r}') \cdot \mathbf{J}(\mathbf{r}') dv', \quad \mathbf{r} \in O. \quad (10)$$

The operators \mathcal{K}_I and \mathcal{K}_O are compact, which means we can use a truncated SVD to approximate them while controlling the error of the approximation. We have

$$\mathcal{K}_I(\mathbf{J}) \approx \mathcal{U}_I \Sigma_I \mathcal{V}_I^\dagger, \quad (11)$$

$$\mathcal{K}_O(\mathbf{J}) \approx \mathcal{U}_O \Sigma_O \mathcal{V}_O^\dagger \quad (12)$$

where, using q terms for \mathcal{K}_I

$$\begin{aligned} \mathcal{U}_I(a) &= \sum_{i=1}^q a_i \mathbf{u}_i^I, \quad \mathbf{u}_i^I \in L_2(S) \\ \Sigma_I &= \text{diag}(\sigma_1^I, \sigma_2^I, \dots, \sigma_q^I) \\ \mathcal{V}_I^\dagger(\mathbf{f}) &= \left[(\mathbf{v}_1^I, \mathbf{f})_I, (\mathbf{v}_2^I, \mathbf{f})_I, \dots, (\mathbf{v}_q^I, \mathbf{f})_I \right]^T \end{aligned} \quad (13)$$

and using p terms for \mathcal{K}_O

$$\begin{aligned} \mathcal{U}_O(a) &= \sum_{i=1}^p a_i \mathbf{u}_i^O, \quad \mathbf{u}_i^O \in L_2(O) \\ \Sigma_O &= \text{diag}(\sigma_1^O, \sigma_2^O, \dots, \sigma_p^O) \\ \mathcal{V}_O^\dagger(\mathbf{f}) &= \left[(\mathbf{v}_1^O, \mathbf{f})_S, (\mathbf{v}_2^O, \mathbf{f})_S, \dots, (\mathbf{v}_p^O, \mathbf{f})_S \right]^T. \end{aligned} \quad (14)$$

As in the matrix SVD, the norm of the error committed in the aforementioned truncation is bounded by the norm of the vector of discarded singular values. Hence, the error can be estimated by computing, say, twice as many singular values than intended. If the norm of the second half of the singular values vector is small enough compared to that of the first half, the order may be deemed high enough and, if not, more singular values should be computed. The appropriate tolerance for determining the truncation order depends on the accuracy required for the specific application. For the MRI example described in this paper, we increased the order until the norm of the second half was a thousand times smaller than the norm of the first half (see Section V-B).

To obtain an approximate SVD of \mathcal{T} , we insert (11) and (12) into (5)

$$\mathcal{T} \approx \mathcal{U}_O \underbrace{\Sigma_O \mathcal{V}_O^\dagger \mathcal{L}^{-1} \mathcal{U}_I \Sigma_I \mathcal{V}_I^\dagger}_M \quad (15)$$

and compute an SVD of the matrix M , marked by the brace in (15)

$$M = U_M \Sigma_M V_M^\dagger \quad (16)$$

where the \dagger denotes the conjugate transpose. Replacing the term marked by the brace in (15) by its SVD, (16), we obtain an approximate SVD of \mathcal{T}

$$\begin{aligned} \mathcal{T} &\approx \mathcal{U}_T \Sigma_M \mathcal{V}_T^\dagger \\ \mathcal{U}_T &= \mathcal{U}_O U_M \\ \mathcal{V}_T^\dagger &= V_M^\dagger \mathcal{V}_I^\dagger. \end{aligned} \quad (17)$$

Since the numerical rank of \mathcal{T} is no larger, and potentially smaller than that of either \mathcal{K}_I or \mathcal{K}_O , it may be possible to truncate (17) further without incurring significant errors in the approximation of \mathcal{T} . Indeed, from (15), one can expect the singular values of M to behave roughly like the product $\Sigma_O \Sigma_I$, decaying faster than each one individually.

The point of the aforementioned derivation is clarified by the following final step. We use (11) and (12) to write \mathcal{U}_T and \mathcal{V}_T^\dagger in an alternate form

$$\begin{aligned} \mathcal{U}_T &= \mathcal{K}_O \mathcal{V}_O \Sigma_O^{-1} U_M, \\ \mathcal{V}_T^\dagger &= V_M^\dagger \Sigma_I^{-1} \mathcal{U}_I^\dagger \mathcal{K}_I \end{aligned} \quad (18)$$

where \mathcal{U}_I^\dagger is the operator adjoint to \mathcal{U}_I , and is defined analogously to \mathcal{V}_I in (13). This form is suitable for computation because applying Σ_O^{-1} , Σ_I^{-1} , U_M , and V_M is easy since these are just matrices, and applying \mathcal{V}_O and \mathcal{U}_I only involves distributions defined over region S , and applying \mathcal{K}_O and \mathcal{K}_I only involves computing fields due to sources in free space.

If the singular vectors defined in region S are known exactly, there is no approximation involved in using (18) to compute inner products with singular vectors defined in regions I and O . This is because the truncation error committed in (11) and (12) is orthogonal to the retained vectors. More precisely, define the truncation error operator, say for \mathcal{K}_I , by $\mathcal{E}_q = \mathcal{K}_I - \mathcal{U}_I \Sigma_I \mathcal{V}_I^\dagger$. Then

$$(\mathbf{v}_i^I, \mathbf{f})_I = \frac{1}{\sigma_i^I} (\mathbf{u}_i^I, \mathcal{K}_I \mathbf{f})_S - \frac{1}{\sigma_i^I} (\mathbf{u}_i^I, \mathcal{E}_q \mathbf{f})_S \quad (19)$$

but the last term is identically zero because $(\mathbf{u}_i^I, \mathbf{u}_j^I)_S = 0$ for all $j > i$. Hence, the region I inner product on the left-hand side of (19) can be replaced by the (first) region S inner product on the right-hand side. If these integrals are evaluated numerically, the error incurred is independent of the truncation order q . A similar argument applies to the truncation of \mathcal{K}_O .

In practice, the singular vectors defined in region S are not known exactly. But as explained in Section IV-A, it is possible to use RSVD techniques, together with a set of basis functions for region S , to compute discretized approximations to these singular vectors as well as to the singular values, the σ_i^O and σ_i^I . Once we have these, we form the matrix M by solving q scattering problems (or p adjoint scattering problems if $p < q$), compute an SVD of M , and use it to form the operators \mathcal{U}_T and \mathcal{V}_T according to (18).

III. EVALUATING THE ROM

The steps for evaluating the ROM once it has been constructed with the approach above are as follows.

- 1) Compute the free-space field due to the sources in region I at observation points in region S .

- 2) Compute the inner products of this field with the \mathbf{u}_i^f .
- 3) Multiply a vector of these inner products by the matrix $\Sigma_O^{-1} U_M \Sigma_M V_M^\dagger \Sigma_I^{-1}$.
- 4) Use the result of the last step to form a weighted combination of the \mathbf{v}_i^O .
- 5) Compute the free-space field due to this weighted combination at observation points in region O .

If the scatterer is a complex object, the number of basis functions in region S , denoted by N_S , will be large and computing the free-space fields and inner products above will be time-consuming.

To expedite the ROM evaluation, we replace the full inner products by sampled inner products, along the lines of a recently proposed DEIM.

The main idea in the DEIM is that if we are trying to approximate a vector by a weighted combination of a few orthonormal basis vectors, we need not resort to the full inner products. If the vector to be approximated is in the span of the basis vectors, or almost so, then selecting a few entries in the vector and determining the coefficients based solely on these entries usually suffices. If we choose the number of entries equal to the number of basis vectors, we obtain the DEIM, which is an interpolation method. We may also use more entries than basis vectors to obtain a closer approximation of the full inner products. The DEIM includes an algorithm for selecting the entries, given in the Appendix. Using this idea, we can restrict the computation of the inner products to a small set of points in region S and so expedite the ROM evaluation.

We detail the procedure for the \mathcal{V}_T^\dagger operator; a similar procedure is used for the \mathcal{U}_T operator. To evaluate $\mathcal{V}_T^\dagger(\mathbf{J})$ using (18) involves computing a vector of coefficients $\alpha \in \mathbb{C}^q$ so that

$$\mathcal{V}_T^\dagger(\mathbf{J}) = V_M^\dagger \Sigma_I^{-1} \alpha, \quad (20)$$

where α is given by $\alpha = \mathcal{U}_I^\dagger \mathcal{K}_I(\mathbf{J})$. To compute α , one way would be to use the large set of N_S basis functions for region S . In this basis, the \mathbf{u}_i^f are represented by a $N_S \times q$ matrix U_I , the field $\mathcal{K}_I(\mathbf{J})$ is represented by a $N_S \times 1$ vector $k_I(\mathbf{J})$, and then $\alpha \approx U_I^\dagger k_I(\mathbf{J})$. Note that k_I is a semi-discrete operator that maps a continuous distribution in region I to a column vector of size N_S .

To expedite the computation of α , we approximate it using only $r_I \ll N_S$ entries of $k_I(\mathbf{J})$, which are chosen according to the DEIM. Using a selection matrix, F_I , composed of r_I columns of the $N_S \times N_S$ identity matrix, the chosen entries are written as $F_I^T k_I(\mathbf{J})$, and α is determined approximately by

$$\alpha \approx \tilde{\alpha} = X_I F_I^T k_I(\mathbf{J}) \quad (21)$$

where $X_I = (F_I^T U_I)^{-1}$. By applying a similar procedure for \mathcal{U}_O , we obtain an $N_S \times r_O$ selection matrix F_O , an $N_S \times p$ matrix V_O of output basis vectors, and a semi-discrete operator \mathcal{K}_O that maps N_S coefficients of the basis functions in region S to electric fields at observation points in region O . We denote the DEIM interpolation matrix for the output region by $X_O = (F_O^T V_O)^{-1}$.

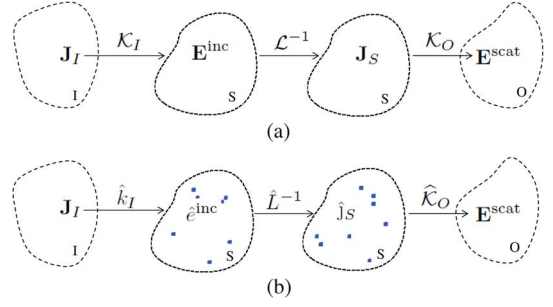


Fig. 2. Full-order (a) and reduced-order (b) models.

Combining the DEIM with the SVD-based ROM, we obtain a new ROM which is of the same order, but much faster to evaluate. The system relating the ROM inputs and outputs is

$$\text{Input : } e^{\text{inc}} = \hat{k}_I(\mathbf{J}_I), \quad (22)$$

$$\text{State equation : } \hat{j}_S = \hat{L}^{-1} e^{\text{inc}}, \quad (23)$$

$$\text{Output : } \mathbf{E}^{\text{scat}} \approx \hat{\mathcal{K}}_O(\hat{j}_S) \quad (24)$$

where

$$\begin{aligned} \hat{k}_I(\mathbf{J}_I) &= F_I^T k_I(\mathbf{J}_I), \\ \hat{L}^{-1} &= X_O^\dagger \Sigma_O^{-1} \left(U_M \Sigma_M V_M^\dagger \right) \Sigma_I^{-1} X_I \\ \hat{\mathcal{K}}_O(a) &= \hat{\mathcal{K}}_O(F_O a). \end{aligned} \quad (25)$$

The inverse of the system matrix \hat{L}^{-1} can be precomputed offline by solving the q scattering problems for each of the \mathbf{u}_i excitations. In (25), the SVD-factored form of M , in parenthesis, includes only the first r_M singular values and vectors of M . The form of full-order and reduced-order models is summarized pictorially in Fig. 2

IV. NUMERICAL IMPLEMENTATION

The procedure for constructing the ROM consists of four steps as follows.

- 1) Use the SVD to obtain a compressed representation of the k_I and \mathcal{K}_O operators.
- 2) Use the DEIM to determine input and output interpolation points.
- 3) Solve the scattering problem for a set of excitations spanning the range of k_I .
- 4) Form matrix M , according to (15), and compress it using the SVD.

Implementation details regarding these steps are given below.

A. Compression of the k_I and \mathcal{K}_O Operators

The operators k_I and \mathcal{K}_O are semi-discrete, that is, they map continuous distributions to discrete column vectors or vice-versa. Computing their full SVDs is challenging, but for our purposes, we only need the singular values and the U_I and V_O matrices. To obtain them, we use an RSVD technique [22].

We apply k_I and \mathcal{K}_O to a set of N_R random excitations. For example, for k_I , these excitations are N_I elementary dipoles with random amplitudes and orientations, distributed in region I . We obtain N_R column vectors representing fields in region S , which we orthonormalize to obtain an $N_S \times N_R$ unitary matrix Q . Then, considering the columns of Q to represent sources in region S , we compute the fields due to these sources at the dipole points in region I . We obtain an $N_R \times N_I$ matrix B , which we compute the SVD of

$$B = U_B \Sigma_B V_B^\dagger \quad (26)$$

and approximate $\Sigma_I \approx \Sigma_B$ and $U_I \approx QU_B$. An analogous procedure is used for \mathcal{K}_O .

As long as N_R is kept moderate, the computational cost of the SVDs is not too high, since the matrices have rank $< N_R$. Of the computed singular values, numerical experiments show that roughly the first half are accurate, and accuracy deteriorates in the second half. Hence, if q singular values are to be retained, we must have $N_R > 2q$. We begin with an estimate of q and N_R , and an error tolerance, and compute the RSVD as described. If the smallest singular value in the first half of singular values is smaller than the error tolerance, the RSVD is considered accurate enough for our purpose. If not, we increase N_R and repeat the RSVD procedure. Once we obtain an adequately accurate SVD, we set q to the smallest value that still guarantees that the error tolerance is met and retain the first q singular values of Σ_B and their corresponding columns of U_I .

B. Generation of Interpolation Points

Our implementation of the DEIM differs slightly from that introduced in [10]. For simplicity, we only describe the procedure for k_I ; the one for \mathcal{K}_O is analogous. The standard approach is to apply DEIM to the truncated basis with q vectors, which yields q interpolation points. This works well when the vector to be approximated is very close in norm to a vector in the column span of the q basis vectors. But if this is not the case (because we allow for a moderate error tolerance) using the standard DEIM introduces fairly large errors.

To overcome this problem, we use more field evaluation points than basis vectors. To generate these points, we take advantage of the RSVD computation and apply the DEIM to the intermediate orthonormal basis $Q^\dagger U_B$ before truncation. We obtain N_R interpolation points which we use to form the matrix $X_I = (F_I^T U_B)^{-1}$, which we then truncate, retaining only its first q rows.

It is important to keep the number of interpolation points moderate, since the cost of evaluating the ROM scales linearly with this number. However, it is possible to use three times as many interpolation points with little overhead, by using all three components of the field at a given point. The DEIM selects basis functions in region S , but, typically, there are three basis functions with overlapping supports, one for each Cartesian component. So we augment the set of basis functions chosen by DEIM with all of the basis functions whose support overlaps that of the chosen set.

To summarize, the combined RSVD+DEIM approach is given in the MATLAB-style code in Algorithm 1.

Algorithm 1 Combined RSVD+DEIM Implementation

```

1: set  $N_R$  number of random excitations
2: set  $q$  number of singular vectors computed,  $2q < N_R$ 
3: set error tolerance  $\tau$ 
4:  $N_I$  and  $N_S$  are the number of basis functions in regions
    $I$  and  $S$ , respectively.
5:  $R = \mathbf{rand}(N_I, N_R)$ 
6:  $R_S = \mathbf{zeros}(N_S, N_R)$ 
7: FOR  $k = 1 : N_R$ 
8:    $R_S(:, k) = k_I(R(:, k))$ 
9: END
10:  $[Q \ R] = \mathbf{qr}(R_S)$ 
11:  $B = \mathbf{zeros}(\mathbf{size}(Q, 2), N_I)$ 
12: FOR  $k = 1 : \mathbf{size}(Q, 2)$ 
13:    $v = k_I^\dagger(Q(:, k))$ 
14:    $(k_I^\dagger(J))$  is just the field due to  $\mathbf{conj}(J)$ , evaluated in
   region  $I$ 
15:    $B(k, :) = v^T$ 
16: END
17:  $[U_B \ \Sigma_B \ V_B] = \mathbf{svd}(B)$ 
18:  $U_B = Q^\dagger U_B$ 
19:  $F_I = \mathbf{deim}(U_B)$ 
20:  $X = (F_I^T U_B)^{-1}$ 
21: FOR  $k = 1 : \mathbf{size}(\Sigma_B)$ 
22:   IF  $\Sigma_B(k, k) < \tau$ 
23:      $q = k$ , BREAK
24:   END
25: END
26:  $U_I = U_B(:, 1 : q)$ 
27:  $\Sigma_I = \Sigma_B(1 : q, 1 : q)$ 
28:  $X_I = X(1 : q, :)$ 
29: RETURN  $U_I, \Sigma_I, X_I, F_I$ .
```

C. Generation and Compression of the Matrix M

Generating the matrix M is typically the most computationally-intensive step. It requires the solution of a scattering problem for each basis excitation, and we assume that the scatterer is such that a direct inversion of \mathcal{L} is not practical. The

excitations can be either the q columns of U_I or the p columns of V_O , whichever is smaller. If $p < q$, the operator \mathcal{L} is replaced by its adjoint, and the results are conjugated and transposed.

Although it is a computational-intensive step, it is embarrassingly parallelizable in shared and distributed memory environments. Hence, an almost linear speedup can be expected when using up to q cores or machines.

Once the matrix M is formed, according to (15), we compute its SVD and discard singular values (and corresponding singular vectors) which are below a given error tolerance. The matrix M can then be stored and applied in its SVD-factored form. In practice, however, if q is not too large, this last step is not essential.

D. Summary of Key Features

The most notable features of the proposed approach are as follows.

- The compression of the input and output operators is purely algebraic, and only depends on the geometry of regions I , O , and S .
- Any electromagnetic solver can be used to solve the scattering problem for the basis excitations.
- The ROM is valid for any source and observation points in regions I and O , and the position of such points is unconstrained within these regions.
- The ROM can be readily and efficiently reused for any configuration of antennas and scatterers within regions I and O , and combined with any integral equation solver.

V. NUMERICAL RESULTS

A. Problem Specification

We demonstrate the proposed method by applying it to a problem relevant to the design of antennas used in high-field, parallel-transmit, magnetic resonance imaging (MRI) scanners. In these scanners, an array of antennas placed close to the human body is used to excite atoms at the so-called *Larmor frequency*. For the case we consider here, this frequency is 298.2 MHz. Because of the proximity of the human body to the antennas, its presence has to be taken into account when designing the antennas and the RF transmission network. Analyzing the interaction of the antennas with the human body is computationally intensive, especially if the body is to be modeled realistically, and this makes it hard to optimize a design, or assess its sensitivity to changes in the body's position.

The human model we use is the highly realistic and inhomogeneous DUKE model of the virtual family [23], of which we use only the head and shoulders (Fig. 3). This is a voxel-based model, in which the complex permittivity is defined on a uniform grid of 5-mm resolution. We define the input and the output regions to be a cylindrical shell around the head, between 140 and 160 mm from the center of the head, and with a vertical length of 220 mm. The antennas may reside anywhere in this region. Since the model is defined at voxels, we use a voxel-based method for the solver. We use an electric-field volume integral equation (EFVIE) method with pulse basis functions similar to that of [24], but with a better conditioned formulation to be described elsewhere [25]. The head model is embedded in a cuboid

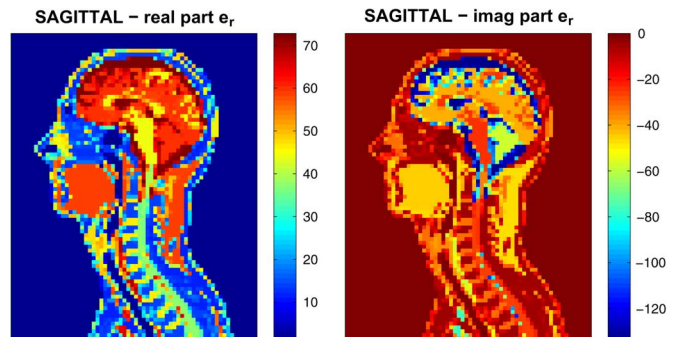


Fig. 3. Sagittal views of the (top) real part and (bottom) imaginary part of ϵ_r for the 5-mm resolution Duke model at 298.2 MHz.

domain of lengths 320 mm \times 480 mm \times 400 mm, uniformly discretized into 5-mm resolution voxels. This domain has 491520 voxels and three times as many basis functions. Of these, region S contains $N_S = 98339$ voxels and regions I and O contain $N_I = 26784$ voxels.

B. ROM Construction

Since regions I and O are the same, the procedure is simpler than in the general case. We have $V_O^\dagger = U_I$ and, therefore, we also use the same set of DEIM points for input and output regions. For the random excitations, we use all of the voxels in region I , and in each one, we have a spatially constant current distribution. While in general, the random excitations could be confined to the surface of region I . Here we use the FFT to generate the incident fields, so using volume current distributions is convenient. We use $N_R = 2000$ random excitations in the I region, and a relative tolerance of $\tau = 0.001$ for the RSVD truncation. Algorithm 1 generates an incident basis of $q = 476$ vectors and 840 interpolation points in the scatterer. The basis is stored in $U_I \in \mathbb{C}^{295017 \times 476}$, and the DEIM matrix in $X_I \in \mathbb{C}^{2520 \times 476}$ (recall that we have three components for each voxel). Due to the proximity of the potential antenna positions to the scatterer (less than 20 mm at the closest point), the number of vectors that we need to keep is relatively high (476), but it is still a small number when compared to the degrees of freedom (DOFS) in regions I (80352) and S (295017). We use the EFVIE solver to solve for each of the 476 vectors contained in the columns of U_I , and form the matrix M . As presented in (16), an SVD is applied to matrix M , and its factorized form is truncated, retaining the 327 largest singular values and corresponding singular vectors. After this truncation, matrix \hat{L}^{-1} in (25) can be represented as the product of a 2520×327 matrix, a diagonal 327×327 matrix, containing the singular values of M , and a 327×2520 matrix. The complete ROM construction takes approximately 4 h on a server equipped with a GPU, with the solution of the 476 scattering problems taking most of the time.

C. Results

The top plot of Fig. 4 depicts a 3-D view of the $N_S = 98339$ voxels in region S (DUKE model, in blue) and $N_I = 26784$ voxels in the input region I (antenna region, in gray) used for the ROM generation. The bottom plot of Fig. 4 shows the same

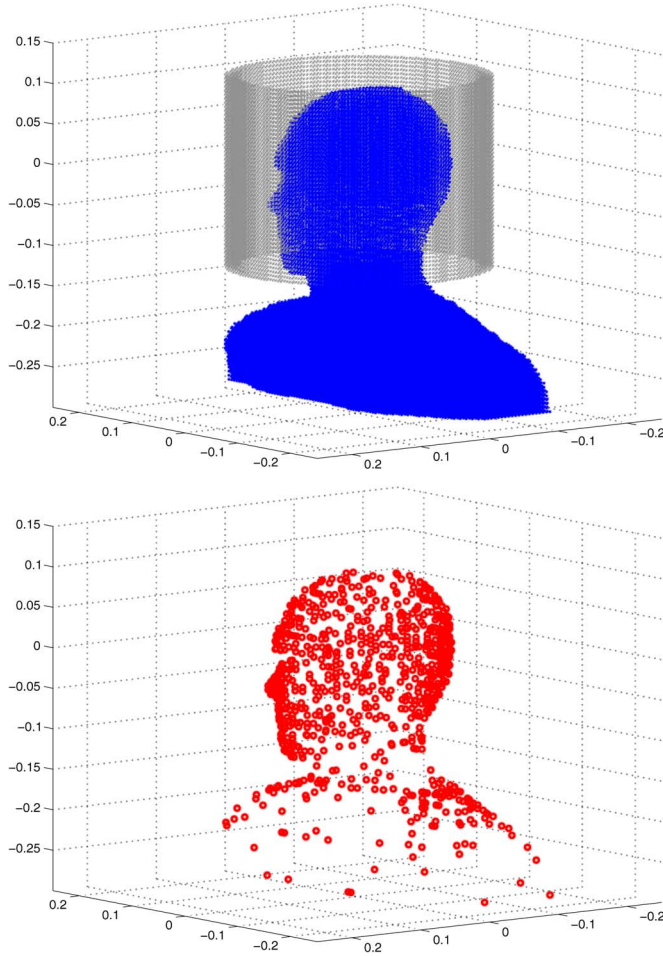


Fig. 4. (Top) 3-D view of the voxels in the DUKE model (in blue) and in the antenna region (in gray). (Bottom) voxels selected by the DEIM for the interpolation (in red).

TABLE I
RESULTS FOR 100 RANDOM EXCITATIONS

	EFVIE solver	Projection	DEIM
Interpolation Points	-	98339	840
Av. Time (s)	25.09*	3.37	0.11
$R_2(e^{\text{inc}})$	0	3.09e-3	3.21e-3
$R_2(e^{\text{scat}})$	0	6.24e-4	7.31e-4

* EFVIE times use a GPU-accelerated code.

3-D domain in which the DUKE model has been replaced by the 840 interpolation points selected by Algorithm 1.

D. Approximation of the Incident Field

To test the approximation of $\hat{e}^{\text{inc}} = k_I(\mathbf{J})$, we compare the approximation obtained using the DEIM points with that obtained using all points, and with the exact $k_I(\mathbf{J})$. The relative 2-norm errors

$$R_2(e^{\text{inc}}) = \frac{\|\tilde{e}^{\text{inc}} - \hat{e}^{\text{inc}}\|_2}{\|\hat{e}^{\text{inc}}\|_2} \quad (27)$$

are shown in Table I. In (27), $\tilde{e}^{\text{inc}} = U_I \alpha$ is the approximation of the field due to the random excitations, and \hat{e}^{inc} is the exact field, discretized using the region S basis functions. When the DEIM points are used, $\alpha = X_I F_I^T \hat{e}^{\text{inc}}$, and when all of the

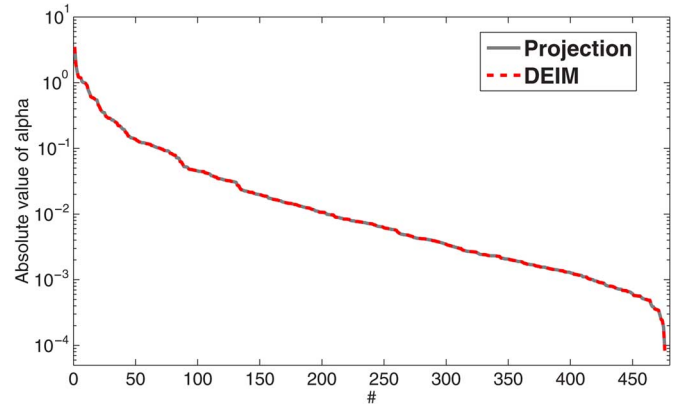


Fig. 5. Comparison of the α_i coefficients obtained using the DEIM points and all of the points.

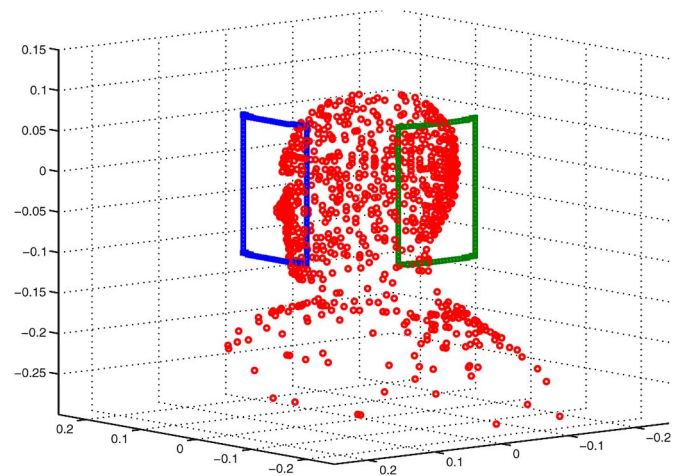


Fig. 6. The 3-D view of the DEIM points (in red) for the DUKE model, with the voxels associated with a transmitting coil (blue), and the voxels associated with a receiving coil (green).

points are used, $\alpha = U_I^\dagger \hat{e}^{\text{inc}}$. The same formulas are used to characterize the error for the scattered field \mathbf{E}^{scat} .

Table I presents the worst case results among the results obtained for 100 random current distributions in the I region. The absolute values of the 476 coefficients in α are shown in Fig. 5, for a square loop of uniform current (Fig. 6). As can be observed, the α_i computed using the DEIM points matches those computed using all of the points to a high degree.

E. Scattered Field Approximation

For each of the 100 random current distributions in region I , we compute the scattered field in region O (which is the same region in this case). Again, we compare errors using only the DEIM points, all of the points, and the EFVIE solver. Table I also includes the average time per excitation required by each method.

In a second setting, we place a loop of uniform current in region I as a rough model for a transmitting antenna. The voxels associated with the transmitting and receiving coils are shown in Fig. 6, in blue and green, respectively. We compute the scattered field at a receiving coil located in a different position in region I , and the results of this computation are shown in Fig. 7, where the high accuracy of the ROM approximation can be readily observed.

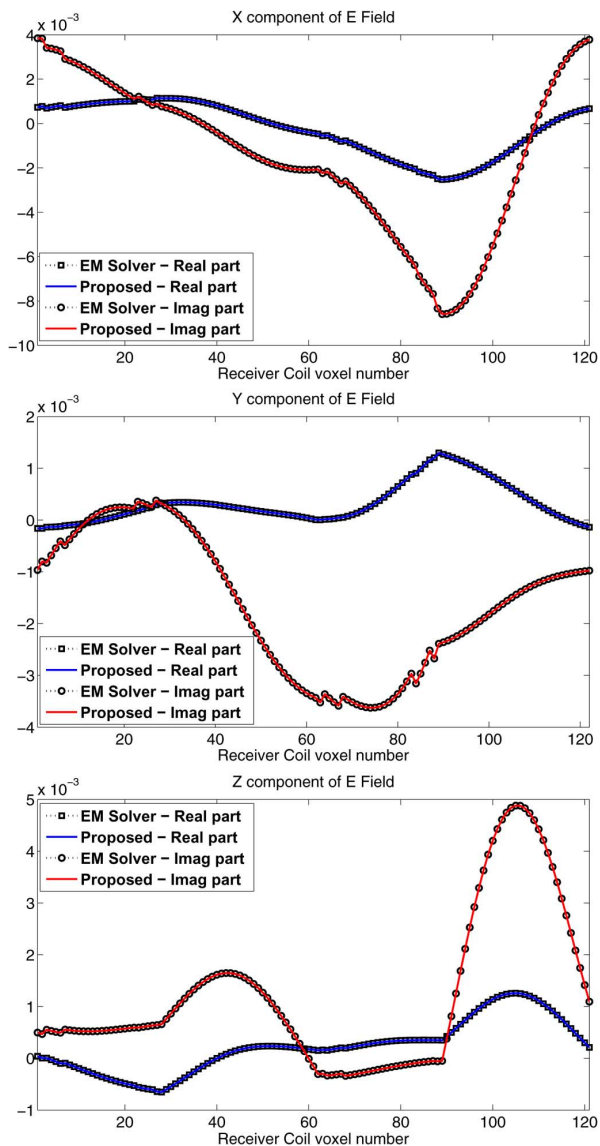


Fig. 7. From top to bottom: real and imaginary parts of the X , Y , and Z components of the scattered electric field at the receiving coil voxels, using the EFVIE solver and the proposed ROM.

F. Combination With a Thin-Wire MoM Solver

The proposed ROM can be particularly useful when combined with an integral-equation solver, since it can be used to model a simpler scatterer or antenna in the vicinity of the scatterer modeled by the ROM.

To demonstrate this possibility, we use a very simple MoM solver for thin-wire structures [26]. We place a circular wire loop antenna in region I . The loop has a radius of 74.5 mm, a wire diameter of 1 mm, and it is discretized into 94 segments of approximately 5 mm each (Fig. 8). The loop dimensions were chosen so that its resonance is close to the frequency of interest 298.2 MHz. The wire loop is placed at $d = 147.5$ mm away from the center of the head (less than 20 mm away from the closest head voxel), and it is excited at 298.2 MHz using a delta gap source at the top of the loop. The choice of the distance to the head is such that no coil element coincides in space with the elements that were used to generate the ROM.

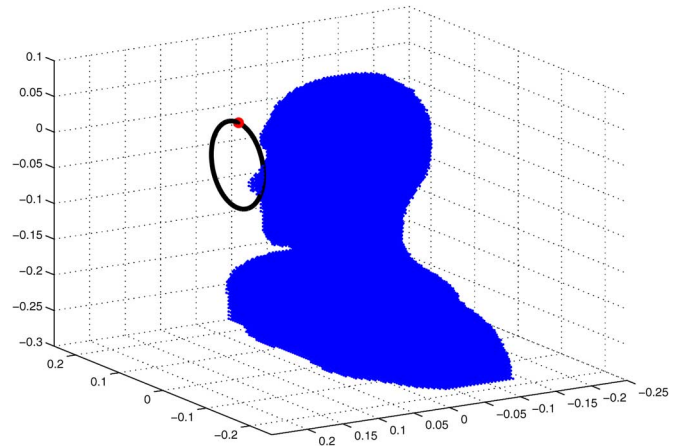


Fig. 8. The 3-D view of the DUKE model (in blue) and the circular wire-loop antenna.

TABLE II
IMPEDANCE OF THE WIRE-LOOP ANTENNA

	Time (s)	$Z _1$ (Ω)	$Z _2$ (Ω)
MoM (no head)	0.06	35011.1+j 12172.1	35011.1+j 12172.1
MoM + EFVIE*	2809.25	32582.1+j 5636.9	37078.2+j 12470.1
MoM + ROM	0.48	32543.0+j 5653.7	36960.4+j 12486.9

$Z|_1$ is for $d = 147.5$ mm, $Z|_2$ is for $d = 167.5$ mm.

* MoM + EFVIE times use a GPU-accelerated code.

In the thin-wire MoM model, the loop current is discretized into segments of constant current, and the vanishing of the tangential component of the electric field is enforced at the centers of the segments. In the absence of the head, this leads to a linear system

$$v = Z_0 i \quad (28)$$

where i is the vector of unknown segment currents, v is a vector of voltages due to the delta-gap source, and Z_0 is a generalized impedance matrix. With the ROM available, this equation is easily modified to take into account the presence of the head. We have

$$v = (Z_0 - G^T X_O \Sigma_O^{-1} M \Sigma_I^{-1} X_I G) i \quad (29)$$

where G is a 2520×94 matrix that maps the current moments of the segments forming the loop to the discretized electric fields they produce at the DEIM elements in the head. Exploiting reciprocity, the transpose of this matrix is used to map the current moments at the DEIM points to the electric field (multiplied by segment length) they produce at the antenna segments. Finally, the minus sign in (29) is needed to relate an electric field to a voltage.

The system matrix in (29) is obtained very fast, since it only involves generating the matrix G and a few matrix multiplications. We compare this with a more standard approach, where the EFVIE solver is coupled with the thin-wire MoM solver. In this case, the coupling must be computed between each of the 94 segments of the wire loop and the 98339 voxels of the body model. Constructing the 94×94 system matrix involves

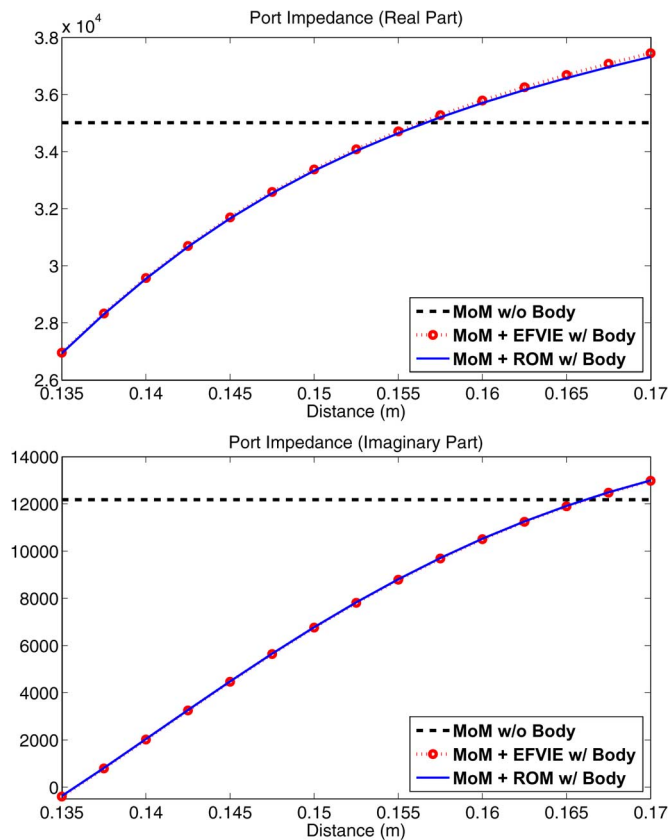


Fig. 9. (Top) Real and (bottom) imaginary parts of the port impedance for a 74.5-mm-loop antenna as a function of the distance from the center of the head, with and without the head.

94 solves using the EFVIE, with takes about 46 min. In this scenario, methods, such as the ACA, could be applied to obtain a compressed version of the coupling between the wire loop and the body model, speeding up the computation. However, any change in the geometry or position of the wire loop would require recomputing the compressed coupling. On the other hand, the proposed ROM can be reused for any geometry or position of the antenna, as long as it fits in the input/output region.

The values of the port impedance with the head present and without it are shown in Table II. In MRI, the loops are electrically small and their port impedance is largely inductive. We choose, however, to make the loop larger in order to increase the effect the head has on the port impedance. The results obtained using the ROM match those obtained with the coupled EFVIE+MOM solver fairly closely (less than 0.2% error), but the latter takes half a second, while the former takes 46 min. Using the ROM, it becomes more practical to automate and optimize the design of an antenna array while controlling the total absorbed power. To test the robustness of the proposed method, we also experimented with placing the antenna at different distances, including positions outside region I . Fig. 9 shows the real and imaginary part of the port impedance with and without the head as the loop distance varies, from 135 to 170 mm. This includes positions between the region I and the head, as well as positions beyond region I . It is clear that the proposed ROM is able to capture the behavior of the complete system, since it is in fairly good agreement with the results of the MoM+EFVIE. As

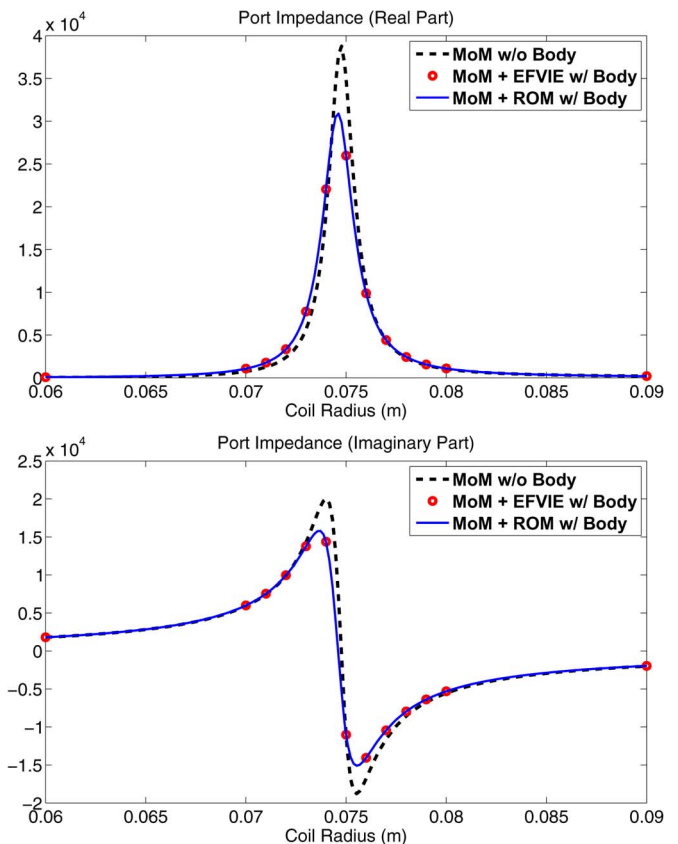


Fig. 10. (Top) Real and (bottom) imaginary parts of the port impedance a loop antenna as a function of the coil radius, when placed at $d = 142.5$ mm, with and without the head.

can be observed in the second column of Table II, when placing the antenna $d = 167.5$ mm away from the center of the head, the ROM is still very accurate (0.3% error in the absolute value).

We now compare the response of the coil loop as we vary the radius, from 60 mm to 90 mm, when placed at $d = 142.5$ mm. The coil is discretized into a varying number of segments (76 for 60 mm to 114 for 90 mm) of approximately 5-mm length. The variation of the real and imaginary parts of the port impedance is shown in Fig. 10, and good agreement between the ROM and the MoM+EFVIE can be observed.

Note that in all of these settings, solving the MoM+EFVIE for each distance or for each coil radius requires approximately 45 min, whereas the solution with the proposed ROM requires half a second per solve.

Finally, the current distribution along the 74.5-mm radius loop when placed at $d = 147.5$ mm, with and without the head, is shown in Fig. 11. Here, too, good agreement between the ROM and the coupled EFVIE+MoM solver is evident.

VI. CONCLUSION

A method for generating ROMs of complex scatterers was described. While we focused on inhomogeneous dielectric scatterers, the approach is general and it can be easily adapted to other types of scatterers. The ROMs are based on the SVD of the operator relating currents in an input region to the electric fields they produce, in the presence of the scatterer, in an output

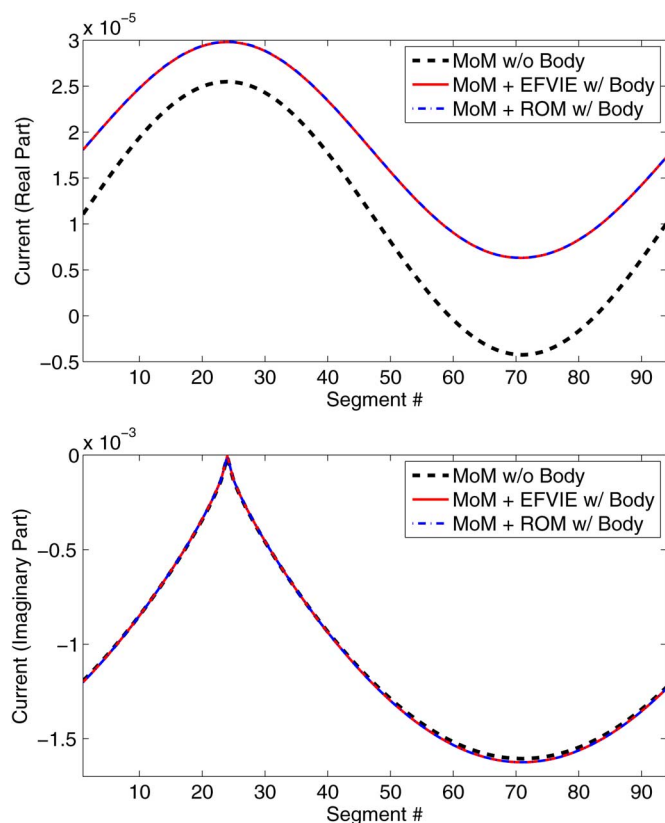


Fig. 11. (Top) real and (bottom) imaginary parts of the currents flowing through each segment of the wire antenna, with and without the head.

region. The models are therefore optimal in the sense that they are the most accurate for a prescribed rank. Despite this optimality, a straightforward application of the SVD involves inner products over 3-D, possibly infinite domains and, hence, it is not practical. We therefore replace these inner products with approximate inner products using the DEIM. The resulting model consists of elementary sources inside the scatterer, with amplitudes determined from the values of the incident field at the source locations. As the number of sources is moderate, the ROM is very fast to evaluate. Once constructed, it can be combined with an integral-equation solver to analyze interactions between antennas, or simple scatterers, and the complex scatterer. As shown in the numerical results section, a loop antenna radiating near a highly realistic human head model can be analyzed accurately in half a second on a desktop PC. This capability enables the automated design and optimization of antennas operating near complex scatterers.

APPENDIX

For completeness, a brief description of the DEIM is given as follows. This description differs from that of [10] in that all quantities are complex, but this modification is straightforward.

Consider approximating a nonlinear vector function $f : \mathbb{R}^M \mapsto \mathbb{C}^N$ and assuming that the range of f is contained, at least approximately, in a linear space spanned by a set of known orthonormal vectors, $U \in \mathbb{C}^{N \times q}$. More precisely

$$f(x) \approx Uc(x), \quad x \in \mathbb{R}^M \quad (30)$$

for some coefficients $c(x) \in \mathbb{C}^q$. The best approximation in the least-squares sense is obtained when $c(x) = U^\dagger f(x)$, but when $N \gg q$, computing all N components of $f(x)$ may be too time consuming. In the DEIM, the q coefficients $c(x)$ are computed by a discrete interpolation, that is, the approximation is forced to be exact for q of the N components of f . The operation of selecting q rows of a length N column vector is expressed using a selection matrix P , which is composed of the corresponding columns of the size N identity matrix. Then, $P^T f(x) \in \mathbb{C}^q$ are the components used to determine the coefficients $c(x)$ and we have

$$c(x) = (P^T U)^{-1} P^T f(x) \quad (31)$$

and inserting this expression into (30), we obtain the DEIM approximation

$$f(x) \approx U(P^T U)^{-1} P^T f(x). \quad (32)$$

The algorithm for selecting the points is a greedy algorithm aimed at minimizing an error bound developed in [10], and it is guaranteed to yield an invertible $P^T U$. Let us denote the indices of the components to be selected by n_1, n_2, \dots, n_q , so that $P^T v = [v_{n_1}, v_{n_2}, \dots, v_{n_q}]$. We first order the columns of U in order of decreasing “importance”, that is, such that $|c(x)|$ will be usually sorted in decreasing order. If, as is usually the case, U was obtained from an SVD, the usual ordering of the U matrix is adequate. In the first iteration, we set n_1 equal to the index of the largest component in the first column of U . Then, we approximate the second column of U by the first column of U times a coefficient, determined in order to make the approximation exact at n_1 . We compute the residue of the approximation, and set n_2 equal to the index at which the residue is largest. We proceed in this way until we have q points. The algorithm is given more precisely in Algorithm 2.

Algorithm 2 DEIM

- 1: Input: U is an $N \times q$ unitary matrix.
 - 2: $n_1 = \arg \max(|U(:, 1)|)$
 - 3: $P = I(:, n_1)$ (I is the order N identity matrix.)
 - 4: **FOR** $i = 2 : N$
 - 5: Solve $(P^T U(:, 1 : i - 1))c = P^T U(:, i)$
 - 6: $r = U(:, i) - U(:, 1 : i - 1)c$
 - 7: $n_i = \arg \max(|r|)$
 - 8: $P(:, i) = I(:, n_i)$
 - 9: **END**
 - 10: **RETURN** P
-

REFERENCES

- [1] A. C. Antoulas, *Approximation of Large-Scale Dynamical Systems*. Philadelphia, PA, USA: SIAM, 2005.

- [2] A. Odabasioglu, M. Celik, and L. T. Pileggi, "PRIMA: Passive reduced-order interconnect macromodeling algorithm," *IEEE Trans. Comput.-Aided Design Integr. Circuits Syst.*, vol. 17, no. 8, pp. 645–654, Aug. 1998.
- [3] J. R. Phillips, L. Daniel, and L. M. Silveira, "Guaranteed passive balancing transformations for model order reduction," *IEEE Trans. Comput.-Aided Design Integr. Circuits Syst.*, vol. 22, no. 8, pp. 1027–1041, Aug. 2003.
- [4] J. D. Geest, T. Dhaene, N. Faché, and D. D. Zutter, "Adaptive CAD-model building algorithm for general planar microwave structures," *IEEE Trans. Microw. Theory Tech.*, vol. 47, no. 9, pp. 1801–1809, Sep. 1999.
- [5] B. Bond, Z. Mahmood, Y. Li, R. Sredojevic, A. Megretski, V. Stojanovic, Y. Avniel, and L. Daniel, "Compact modeling of nonlinear analog circuits using system identification via semidefinite programming and incremental stability certification," *IEEE Trans. Comput.-Aided Design Integr. Circuits Syst.*, vol. 29, no. 8, pp. 1149–1162, Aug. 2010.
- [6] M. Hess and P. Benner, "Fast evaluation of time-harmonic Maxwell's equations using the reduced basis method," *IEEE Trans. Microw. Theory Tech.*, vol. 61, no. 6, pp. 2265–2274, Jun. 2013.
- [7] G. Rozza, D. B. P. Huynh, and A. T. Patera, "Reduced basis approximation and *a posteriori* error estimation for finely parametrized elliptic coercive partial differential equations," *Archives Comput. Meth. Eng.*, vol. 15, no. 3, pp. 229–275, 2008.
- [8] B. Bond and L. Daniel, "Parameterized model order reduction of nonlinear dynamical systems," in *Proc. IEEE/ACM Int. Conf. Comput.-Aided Design*, 2005, pp. 487–494.
- [9] M. Barrault, Y. Maday, N. Nguyen, and A. Patera, "An empirical interpolation method: Application to efficient reduced-basis discretization of partial differential equations," *C. R. Math.*, vol. 339, no. 9, pp. 667–672, 2004.
- [10] S. Chaturantabut and D. C. Sorensen, "Nonlinear model reduction via discrete empirical interpolation," *SIAM J. Sci. Comput.*, vol. 32, no. 5, pp. 2737–2764, 2010.
- [11] A. Hochman, B. Bond, and J. White, "A stabilized discrete empirical interpolation method for model reduction of electrical, thermal, microelectromechanical systems," in *Proc. ACM Design Autom. Conf.*, Jun. 2011, pp. 540–545.
- [12] R. Garbacz and R. Turpin, "A generalized expansion for radiated and scattered fields," *IEEE Trans. Antennas Propag.*, vol. AP-19, no. 3, pp. 348–358, May 1971.
- [13] R. Harrington and J. Mautz, "Theory of characteristic modes for conducting bodies," *IEEE Trans. Antennas Propag.*, vol. 19, no. 5, pp. 622–628, Sep. 1971.
- [14] G. Tayeb and S. Enoch, "Combined fictitious-sources-scattering-matrix method," *JOSA A*, vol. 21, no. 8, pp. 1417–1423, 2004.
- [15] L. Crocco, F. Cuomo, and T. Isernia, "Generalized scattering-matrix method for the analysis of two-dimensional photonic bandgap devices," *JOSA A*, vol. 24, no. 10, pp. A12–A22, 2007.
- [16] A. Hochman, Y. Leviatan, and J. K. White, "On the use of rational-function fitting methods for the solution of 2D Laplace boundary-value problems," *J. Comput. Phys.*, vol. 238, pp. 337–358, 2013.
- [17] L. Matekovits, V. Laza, and G. Vecchi, "Analysis of large complex structures with the synthetic-functions approach," *IEEE Trans. Antennas Propag.*, vol. 55, no. 9, pp. 2509–2521, Sep. 2007.
- [18] S. Chaillat and G. Biros, "Faims: A fast algorithm for the inverse medium problem with multiple frequencies and multiple sources for the scalar Helmholtz equation," *J. Comput. Phys.* vol. 231, no. 12, pp. 4403–4421, 2012. [Online]. Available: www.scopus.com
- [19] M. Bebendorf, "Approximation of boundary element matrices," *Numer. Math.*, vol. 86, no. 4, pp. 565–589, 2000.
- [20] S. Kurz, O. Rain, and S. Rjasanow, "The adaptive cross approximation technique for the 3-D boundary element method," *IEEE Trans. Magn.*, vol. 38, no. 2, pp. 421–424, Mar. 2002.
- [21] K. Zhao, M. Vouvakis, and J. F. Lee, "The adaptive cross approximation algorithm for accelerated method of moments computations of EMC problems," *IEEE Trans. Electromagn. Compat.*, vol. 47, no. 4, pp. 763–773, Nov. 2005.
- [22] N. Halko, P. G. Martinsson, and J. A. Tropp, "Finding structure with randomness: Probabilistic algorithms for constructing approximate matrix decompositions," *SIAM Rev.* vol. 53, no. 2, pp. 217–288, 2011. [Online]. Available: <http://dx.doi.org/10.1137/090771806>
- [23] A. Christ *et al.*, "The Virtual Family—Development of anatomical CAD models of two adults and two children for dosimetric simulations," *Phys. Med. Biol.*, vol. 55, no. 2, pp. N23–N38, 2010.
- [24] D. E. Livesay and K.-M. Chen, "Electromagnetic fields induced inside arbitrarily shaped biological bodies," *IEEE Trans. Microw. Theory Tech.*, vol. MTT-22, no. 12, pp. 1273–1280, Dec. 1974.
- [25] A. G. Polimeridis, J. F. Villena, L. Daniel, and J. K. White, "Stable FFT-JVIE solvers for fast analysis of highly inhomogeneous dielectric objects," *J. Comput. Phys.*, 2013, submitted for publication.
- [26] R. Harrington, "Matrix methods for field problems," *Proc. IEEE*, vol. 55, no. 2, pp. 136–149, Feb. 1967.

Amit Hochman (S'08–M'09) received the B.Sc., M.Sc., and Ph.D. degrees in electrical engineering from the Technion-Israel Institute of Technology, Haifa, Israel, in 1996, 2005, and 2009, respectively.

From 2009 to 2012, he was a Postdoctoral Researcher at the Computational Prototyping Group, Massachusetts Institute of Technology's Research Laboratory of Electronics, Cambridge, MA, USA. He is currently a Research Affiliate with this group. His research interests revolve around computational electromagnetics in various domains: antennas, optics, RF circuits, and signal integrity. He has also worked on model-order reduction for various applications, such as microelectromechanical systems, batteries for electrical vehicles, and nonlinear circuits.

Jorge Fernández Villena was born in Avilés, Spain, in 1980. He received the Ph.D. degree in electrical and computer engineering from Instituto Superior Técnico, T.U. Lisbon, Lisbon, Portugal, in 2010.

From 2005 to 2012, he was a Researcher at the IINESC ID, Lisbon. Currently, he is a Postdoctoral Associate at the Massachusetts Institute of Technology (MIT), Cambridge, MA, USA, working as a Researcher for the Computational Prototyping Group at the Research Laboratory of Electronics. His research interests include the development and implementation of numerical methods and algorithms for analysis and simulation of physical problems encountered in engineering applications.

Athanasios G. Polimeridis (M'04) was born in Thessaloniki, Greece, in 1980. He received the Diploma degree in electrical engineering and the Ph.D. degree in electrical and computer engineering, Aristotle University of Thessaloniki (AUTH), Thessaloniki, Greece, in 2003 and 2008, respectively.

From 2008 to 2012, he was a Postdoctoral Research Associate with the Laboratory of Electromagnetics and Acoustics, Ecole Polytechnique Fédérale de Lausanne (EPFL), Lausanne, Switzerland. Currently, he is a Postdoctoral Research Associate at the Massachusetts Institute of Technology, Cambridge, MA, USA, where he is a member of the Computational Prototyping Group at the Research Laboratory of Electronics. His research interests revolve around computational methods for problems in physics and engineering (electromagnetics, Casimir forces, MRI), with an emphasis on the development and implementation of integral-equation-based algorithms.

Dr. Polimeridis was awarded a Swiss National Science Foundation Fellowship for Advanced Researchers in 2012.

Luís Miguel Silveira (S'85–M'95–SM'00–F'12) was born in Lisbon, Portugal. He received the M.S., E.E., and Ph.D. degrees in electrical and computer engineering from the Massachusetts Institute of Technology, Cambridge, MA, USA, in 1990, 1991, and 1994, respectively.

Currently, he is a Professor and Head of the Department of Electrical and Computer Engineering at Instituto Superior Técnico (IST), University of Lisbon, and a Senior Researcher with Instituto de Engenharia de Sistemas e Computadores, Investigação e Desenvolvimento em Lisboa (INESC ID). His research interests include various aspects of computer-aided design of integrated circuits, with an emphasis on interconnect modeling and simulation, parallel computer algorithms, and the theoretical and practical issues concerning numerical simulation methods for circuit design problems. He has received notable paper citations at various conferences, including ICCAD, DAC, DATE, ECTC, VLSI-SoC, and SBCCI.

Prof. Silveira is a member of Sigma Xi.

Jacob K. White (F'08) received the B.S. degree in electrical engineering and computer science from the Massachusetts Institute of Technology (MIT), Cambridge, MA, USA, in 1980, and the S.M. and Ph.D. degrees in electrical engineering and computer science from the University of California, Berkeley, CA USA, in 1983 and 1985, respectively.

He was with the IBM T. J. Watson Research Center, Yorktown Heights, NY, USA, from 1985 to 1987, was an Analog Devices Career Development Assistant Professor at MIT from 1987 to 1989, and became a Presidential Young Investigator in 1988. Currently, he is a C. H. Green Professor in Electrical Engineering and Computer Science at MIT. He is best known for supervising the development of the interconnect analysis programs Fastcap and Fasthenry; for his collaboration on the development of the algorithms in Spectre and SpectreRF; and for his students' work on linear, nonlinear, and parameterized model reduction. His research interests include numerical algorithms for the simulation and optimization of circuits, interconnect, nanophotonics, bioMEMS and NEMS, bio molecules, and network models of biological systems.

Dr. White was an Associate Editor of the IEEE TRANSACTIONS ON COMPUTER-AIDED DESIGN from 1992 to 1996, and served as the Chair for the International Conference on Computer-Aided Design in 1999.

Luca Daniel received the Laurea degree (Hons.) in electronic engineering from the Università di Padova, Padova, Italy, in 1996, and the Ph.D. degree in electrical engineering from the University of California, Berkeley, CA, USA, in 2003.

He is an Associate Professor in the Electrical Engineering and Computer Science Department, Massachusetts Institute of Technology (MIT), Cambridge, MA, USA. His research interests include accelerated integral equation solvers and parameterized stable compact dynamical modeling of linear and nonlinear dynamical systems with applications in mixed-signal/RF/millimeter-wave circuits, power electronics, microelectromechanical systems, and the human cardiovascular system.

Dr. Daniel received the 1999 IEEE TRANSACTIONS ON POWER ELECTRONICS best paper award, the 2003 ACM Outstanding Ph.D. Dissertation Award in electronic design automation, five best paper awards in international conferences, the 2009 IBM Corporation Faculty Award, and 2010 Early Career Award from the IEEE Council on electronic design automation.